Materials Research Express

PAPER

Bi-functional ZnO nanoparticles as a reusable SERS substrate for nano-molar detection of organic pollutants

Materials Research Express

PAPER

Bi-functional ZnO nanoparticles as a reusable SERS substrate for nano-molar detection of organic pollutants

RECEIVED
30 September 2019

REVISED
16 December 2019

ACCEPTED FOR PUBLICATION
23 January 2020

PUBLISHED
7 February 2020

Bishnu Pada Majee[1], **Bhawna**[1] **and Ashish Kumar Mishra**

School of Materials Science and Technology, Indian Institute of Technology, Banaras Hindu University, Varanasi-221005, India

[1] These authors contributed equally.

E-mail: akmishra.mst@iitbhu.ac.in

Keywords: SERS, ZnO nanoparticles, methylene blue, methyl orange

Abstract

In order to identify the quality of water, detection of organic pollutants at very low concentrations is needed. In this work, hydrothermally grown ZnO nanoparticles (NPs) were used as a SERS active substrate for the detection of nano-molar concentration (10^{-9} M) of Methylene Blue (MB) and Methyl Orange (MO), which is the best known detection limit for any pristine metal oxide nanoparticles as a SERS substrate to detect organic pollutants. Additionally, self cleaning property of used SERS substrate was demonstrated under UV light irradiation in aqueous medium for the reusability of SERS substrate. These cleaned ZnO based SERS substrates were reused to detect the organic pollutant with repeated detectability. Hence, bi-functional behaviour of ZnO NPs is demonstrated in the present work by detection of organic pollutant using ZnO based SERS substrate and self cleaning of SERS substrate for its reusability.

1. Introduction

Surface enhanced Raman spectroscopy (SERS) is a highly precise and sensitive tool for the detection of very tiny amount of molecular species, sometimes close to single molecule level [1–4]. The detection of low concentration of organic pollutants in water bodies is difficult to achieve and necessary for human safety. Methylene Blue (MB) is a thiazine dye and widely used in chemical and biological industries. Similarly, Methyl Orange (MO) is an Azo-dye and widely used in pharmaceutical, chemical and textile industries for the purpose of printing and dyeing. At very low concentrations (micro molar or lower) of these organic pollutants, water is completely colourless and hence their detection through UV–visible absorption spectroscopy is nearly impossible. SERS technique can be used to improve the detection limit up to nano-molar or lower concentrations. In case of SERS, probe molecules get adsorb onto the surface of active substrate giving rise to an enhanced Raman signal due to the chemical and/or electromagnetic enhancement with later as a dominant factor. In general, metal nanostructures show electromagnetic enhancement, while semiconductor nanostructures indicate chemical enhancement. Thus a better detection limit can be achieved using Ag or Au nanoparticles (NPs), however, their high cost restricts their application towards sensing [5–15]. The Ag NPs suffer with oxidation and hence have a limited functional lifetime. Whereas, Au NPs are stable against oxidation but to prevent the formation of their aggregates, usually capping agents are used which hamper the dye adsorption on the surface of Au NPs resulting in reduced Raman signal. In view of this, different metal oxides such as CuO, TiO_2, ZnO etc are being investigated as cost effective alternatives for the detection of different organic pollutants [16–20]. Wang *et al* showed SERS detection of milli-molar concentration of 4-mercaptopyridine using CuO nanocrystal [17]. Gong *et al* performed SERS detection of milli-molar concentration of 4-mercaptobenzoic acid using TiO_2 NPs [18]. The ZnO NPs can be used as SERS active substrates due to their high refractive index, which is helpful in confining the light to enhance the SERS signal. It is used in SERS detection of different organic molecules such as cyanine dye D266, 4-mercaptopyridine (4-MPY), 1,4-bis[2-(4-pyridyl)ethenyl]-benzene (BVPP) and N719 dye [21–24]. Nanocage structure of amorphous ZnO is also studied for efficient SERS detection of 4-mercaptobenzoic acid, 4-mercaptopyridine and 4-aminothiophenol [25]. Adsorption of organic pollutants on the surface of ZnO NPs and charge-transfer between them holds the key in SERS detection of pollutants.

Liu *et al* demonstrated ZnO nanosheets as a SERS substrate to detect the micro-molar concentration of 4-mercaptobenzoic acid [26]. Jin *et al* detected 4-methylpyridine using ZnO nanorods as SERS substrate [27]. Among studies on SERS detection of MB and MO using metal oxides as SERS substrate, detection of milli-molar concentration of MO could be obtained using ZnO nanorods [28]. The detection of milli-molar concentration of MB could be achieved with TiO_2 nanotubes [29], while micro-molar detection was obtained with Niobium pentaoxide NPs [30]. Zhang *et al* demonstrated the detection of MO and MB along with other organic pollutants at 10^{-7} M concentration using MoO_2 nanodumbbells [31]. However, detection of MB and MO at near nano-molar concentration using cost effective pristine metal oxide NPs as SERS substrate is not reported till date to the best of our knowledge.

Here, we successfully demonstrated detection of nano-molar concentrations of both the organic pollutants (MB and MO) using cost effective hydrothermally grown ZnO NPs as SERS substrate. The surface morphology, structure and band gap of prepared ZnO NPs were analyzed using different characterization techniques. The bi-functional behaviour of prepared ZnO NPs was examined by SERS detection of MB and MO at nano-molar concentrations and demonstration of self cleaning behaviour of used SERS substrate under UV irradiation for multiple uses.

2. Experimental

2.1. Materials

Methylene blue trihydrate and Methyl Orange were purchased from Himedia Laboratories Pvt. Ltd, India for the preparation of aqueous solutions of dyes. Zinc acetate dihydrate was purchased from Sisco Research Laboratories Pvt. Ltd, India and methanol was bought from Loba Chemie Pvt. Ltd, India to synthesize the ZnO NPs. These chemicals were used as received without further purification.

2.2. Synthesis of ZnO NPs

To synthesize ZnO NPs, 0.4 M concentration of Zinc acetate dihydrate in methanol (30 ml) was magnetically stirred at room temperature for 30 min. Then the solution was transferred into a teflon lined stainless steel autoclave and maintained at 150 °C inside a hot air oven for 12 h. After completion of reaction time the oven was allowed to cool down to room temperature naturally. Finally, the formed product was air dried for 2 h to obtain pure ZnO NPs [32].

2.3. Preparation of SERS substrate

Aqueous dye solutions of 10^{-5} to 10^{-9} M concentrations were prepared by serial dilution method for both the dyes. SERS substrates were prepared by drop casting method as reported in literature [4, 33, 34]. In this method, 4 mg of ZnO NPs were dispersed in 2 ml respective dye solutions in ultrasonic bath for 30 min for each concentration of MB and MO (10^{-5}, 10^{-6}, 10^{-7}, 10^{-8} and 10^{-9} M). The fixed amount (100 μl) of dispersed solution of ZnO and dye was dropped upon a Si wafer and dried in air at room temperature. These drop casted and dried ZnO/dye over Si were used as SERS substrates.

2.4. Measurement techniques

The surface morphology of the synthesized ZnO NPs was studied using Nova NanoSEM 450 high resolution scanning electron microscope (HRSEM). The structural study was done with a room temperature bench top Rigaku Miniflex 600 x-ray powder diffractometer having a Cu K_α radiation source operating at 40 kV and 15 mA and the Rietveld refinement was done using Full Prof software. The ultraviolet-visible (UV–vis) absorption spectra were recorded on a Biotek UV–vis spectrophotometer and Raman spectra were collected with Airix Corp. STR 300 micro Raman spectrometer having 1200 cm^{-1} grating with step size of 1.2 cm^{-1} and laser source of 532 nm. The SERS spectra of both the dye molecules were recorded for 10 s acquisition time and 3 accumulations with laser power of 0.26 mW at sample. The self-cleaning behaviour of ZnO based SERS substrate was examined for reusability purpose by irradiating ZnO SERS substrate with UV light in presence of DI water using an indigenously designed UV chamber equipped with four UV lamps of 8 W power each.

3. Results and discussion

3.1. Surface morphology and XRD studies

Surface morphology study of synthesized ZnO NPs was done using SEM technique. SEM image (figure 1(a)) of ZnO NPs clearly shows well distributed particles with nearly uniform spheroidal shape. The SEM image indicates the particle size in the range 45–50 nm. It is observed that they are well separated implying higher accessible surface area for better adsorption of dye molecules over ZnO NPs, which is important for their detection. The XRD pattern of ZnO NPs (figure 1(b)) was collected in the 2θ range 20°—70° with a step size of

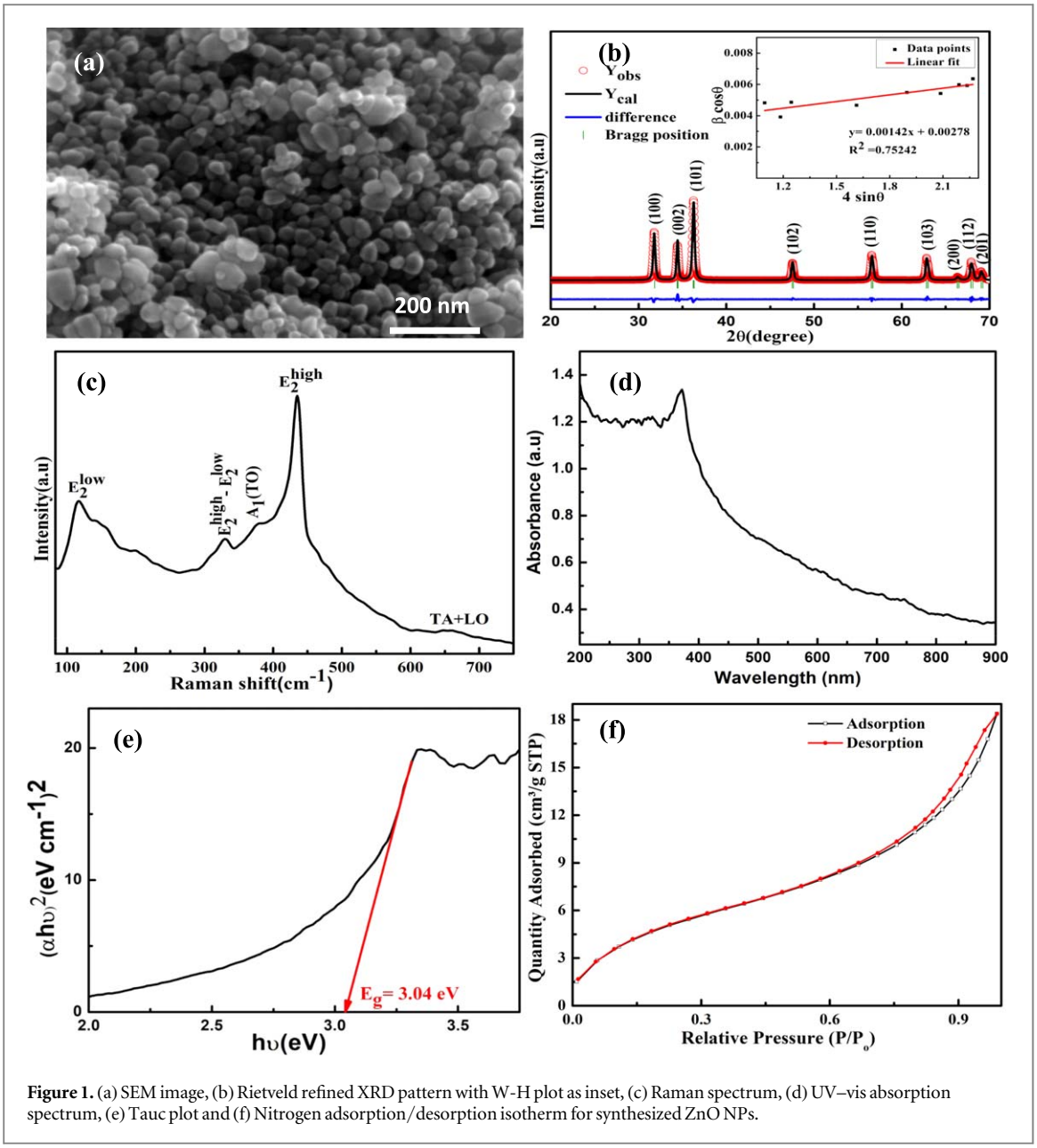

Figure 1. (a) SEM image, (b) Rietveld refined XRD pattern with W-H plot as inset, (c) Raman spectrum, (d) UV–vis absorption spectrum, (e) Tauc plot and (f) Nitrogen adsorption/desorption isotherm for synthesized ZnO NPs.

Table 1. Lattice parameters and crystallite size of ZnO NPs.

Crystalline Parameters (Units)	ZnO NPs
Lattice Parameter (nm)	a = b = 0.32513; c = 0.52083
Unit cell Volume (nm^3)	47.6796
χ^2	3.47
Crystallite size , D(nm)	~50

0.02°. The diffraction peaks are well matched with JCPDS file number (03-065-3411) and absence of any additional peak confirmed the purity of synthesized ZnO. It is found that the formed ZnO NPs have acquired hexagonal wurtzite structure which belongs to the space group $P6_3mc$ having two formula units per primitive cell. The Rietveld refined XRD pattern with pseudo-Voigt function defining the profile shape is utilised to extract the refined cell parameters as tabulated in table 1. The average crystallite size 'D' of the ZnO NPs is determined using the Scherrer formula as given in equation (1) [35].

$$D = k\lambda/\beta_D \cos\theta \quad (1)$$

where k (~0.9) is a dimensionless shape factor, λ is the wavelength of the x-ray radiation, θ is the peak position of Bragg's angle and β_D is the instrument-corrected line broadening at half the maximum intensity (FWHM) which

is evaluated using silicon as standard material [36]. Further, Williamson-Hall (W-H) analysis was performed using equation (2) to incorporate strain induced effects [37]. Therefore,

$$\beta\ cos\theta = (k\lambda/D) + (4\epsilon\ \sin\theta) \quad (2)$$

By plotting $\beta\cos\theta$ with respect to $4\sin\theta$ for all XRD peaks of ZnO-NPs and performing linear fit the value of crystallite size can be calculated from the y-intercept of the fitted line (inset of figure 1(b)). From the y-intercept of W-H plot the size of ZnO NPs is calculated and found to be around 50 nm, which is similar to the SEM measurement.

3.2. Spectroscopic study

The Raman spectrum of synthesized ZnO NPs (figure 1(c)) indicates polar A_1 (TO) mode (~378 cm^{-1}), two non polar modes E_2^{high} (~435 cm^{-1}) and E_2^{low} (~112 cm^{-1}), second order E_2^{high} - E_2^{low} mode (~330 cm^{-1}) and TA + LO mode (~660 cm^{-1}) confirming the formation of wurtzite ZnO. The E_2^{high} and E_2^{low} modes are associated with vibrations of oxygen and vibration of Zn sub-lattice, respectively. Presence of all these peaks confirms the formation of wurtzite ZnO nanostructure as described in literature [38]. In order to perform the band gap study of ZnO NPs, the UV-vis absorption spectrum (figure 1(d)) was recorded in the wavelength range of 200 to 900 nm. A clear peak at around 370 nm is observed suggesting presence of wide band gap in synthesized ZnO NPs. Further, in order to calculate the band gap a Tauc plot was obtained using following equation (3) [39]:

$$(\alpha h\upsilon)^2 = A(h\upsilon - E_g) \quad (3)$$

where α is the absorption coefficient, $h\nu$ is the energy of incident radiation and E_g is the optical band gap. The intercept obtained on the abscissa by extrapolating the linear portion of the $(\alpha h\nu)^2$ versus $h\nu$ graph (figure 1(e)) gives the optical band gap to be around 3.04 eV. Further, surface area analysis was performed to study the porous nature of prepared ZnO NPs. The nitrogen adsorption-desorption isotherm of ZnO NPs is shown in figure 1(f). The obtained specific surface area (using Brunauer–Emmett–Teller, BET method) is found to be around 18.38 $m^2\ g^{-1}$, while pore volume (using Barrett–Joyner–Halenda, BJH method) is obtained to be around 0.024 $cm^3\ g^{-1}$, indicating the porous nature of prepared ZnO NPs. This porous nature of ZnO NPs helps for effective adsorption of dye molecules over its surface, which may lead to the better charge transport between ZnO and dye molecules during SERS process.

The dye molecules were characterized using Raman and UV–vis absorption spectroscopy techniques. Figure 2(a) shows the normal Raman spectra of MB and MO. The Raman peaks of MB around 760 and 1397 cm^{-1} corresponds to C–S–C skeletal deformation and C–H in-plane ring deformation, respectively. Raman peaks around 1170 and 1467 cm^{-1} correspond to out of plane bending and anti-symmetric stretching of C–N mode, respectively. The peak at around 1626 cm^{-1} corresponds to out of plane C–C ring bending [40, 41]. The Raman modes of MO at around 1117 and 1193 cm^{-1} corresponds to Ph–N stretching vibration and the peaks around 1145, 1311 and 1591 cm^{-1} corresponds to C–C stretching vibration. The Raman peaks at around 1390 and 1413 cm^{-1} corresponds to N=N group stretching [42]. The UV–vis absorption spectra of aqueous solutions of MB and MO are shown in figure 2(b). The MO dye shows major absorption in the range 400–500 nm while MB shows major absorption in the range 600–700 nm. In order to calculate the band gap of both the dye molecules, Tauc plots between $(\alpha h\nu)^2$ and $h\nu$ were drawn. The value of band gap of MB comes around 1.81 eV (figure 2(c)) and of MO comes around 2.33 eV (figure 2(d)). The inset of figures 2(c) and (d) clearly indicates that the aqueous solutions of micro molar or lower concentrations of these dye molecules become colorless and would be difficult to detect using UV–vis absorption spectroscopy. Therefore, SERS can be an effective technique to detect such lower concentrations of these organic pollutants.

3.3. SERS analysis

Figures 3(a) and (b) show the SERS spectra for 10^{-5} to 10^{-9} M concentrations of MB and MO adsorbed on ZnO NPs, respectively. The Raman peaks at around 770, 1166, 1394, 1455 and 1626 cm^{-1} in figure 3(a) implies the presence of MB as described in earlier reports [41]. The Raman peaks at around 1117, 1145, 1194, 1312, 1390, 1418 and 1594 cm^{-1} in figure 3(b) implies the presence of MO as described in earlier reports [42]. A significant amount of peak intensity for 1626 cm^{-1} and 1390 cm^{-1} for MB and MO, respectively, is observed even for their lowest concentration at nano-molar level. This clearly indicates the nano-molar detectable limit of ZnO NPs for both the dyes, which is better than earlier reports for any pristine metal oxide nanoparticles to the best of our knowledge. Figure 3(c) shows the linear increase in intensity of 1626 cm^{-1} and 1390 cm^{-1} peaks with concentrations of MB and MO, respectively, acting as a calibration curve for examining the concentration of these dye solutions. Error bars in the calibration curve were calculated using standard deviation based on multiple measurements for same concentration. Lombardi *et al* [43] showed that SERS enhancement of a molecule-semiconductor system depends on many factors such as charge transfer, exciton and molecular resonances. They also observed that the most intense enhancement occurs for transitions terminating at the

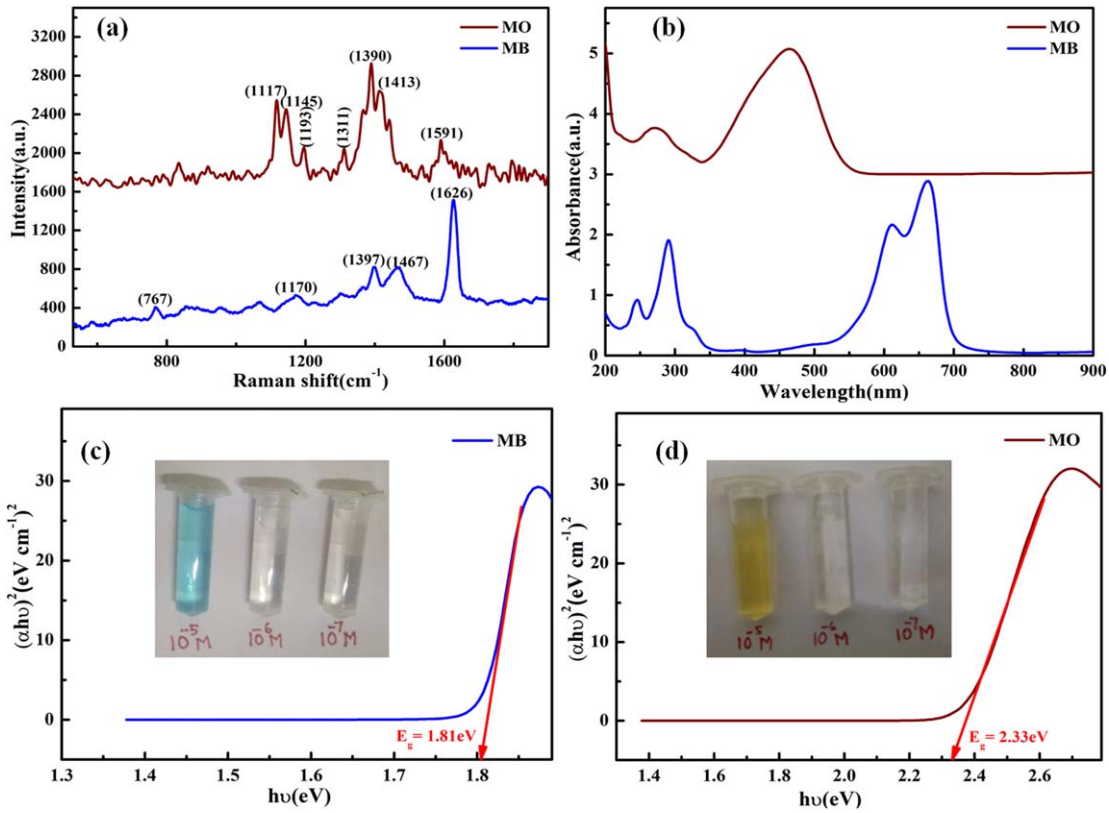

Figure 2. (a) Normal Raman spectra and (b) UV–vis absorption spectra of both dyes, Tauc plot of (c) MB and (d) MO with inset image of their different concentrations (10^{-5}, 10^{-6} and 10^{-7} M).

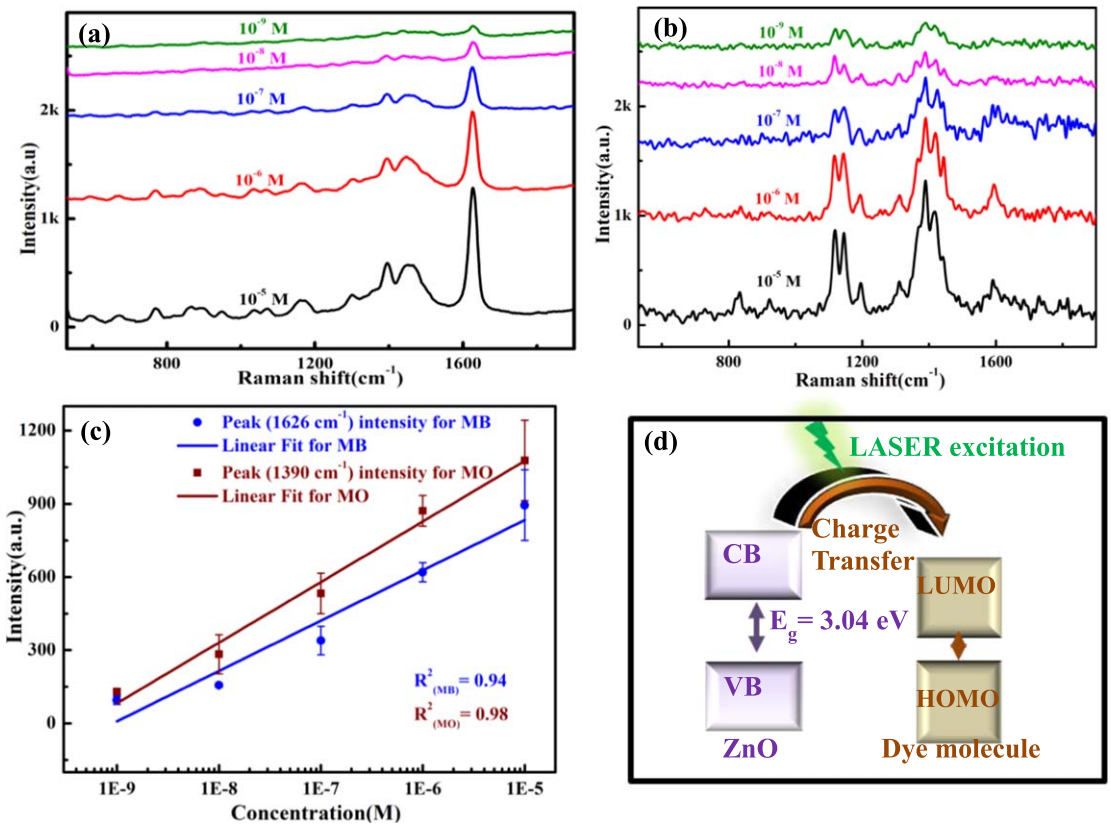

Figure 3. (a) SERS spectra for MB adsorbed ZnO NPs, (b) SERS spectra for MO adsorbed ZnO NPs, (c) SERS intensity versus dye concentration and (d) Schematic for charge transfer mechanism for SERS process.

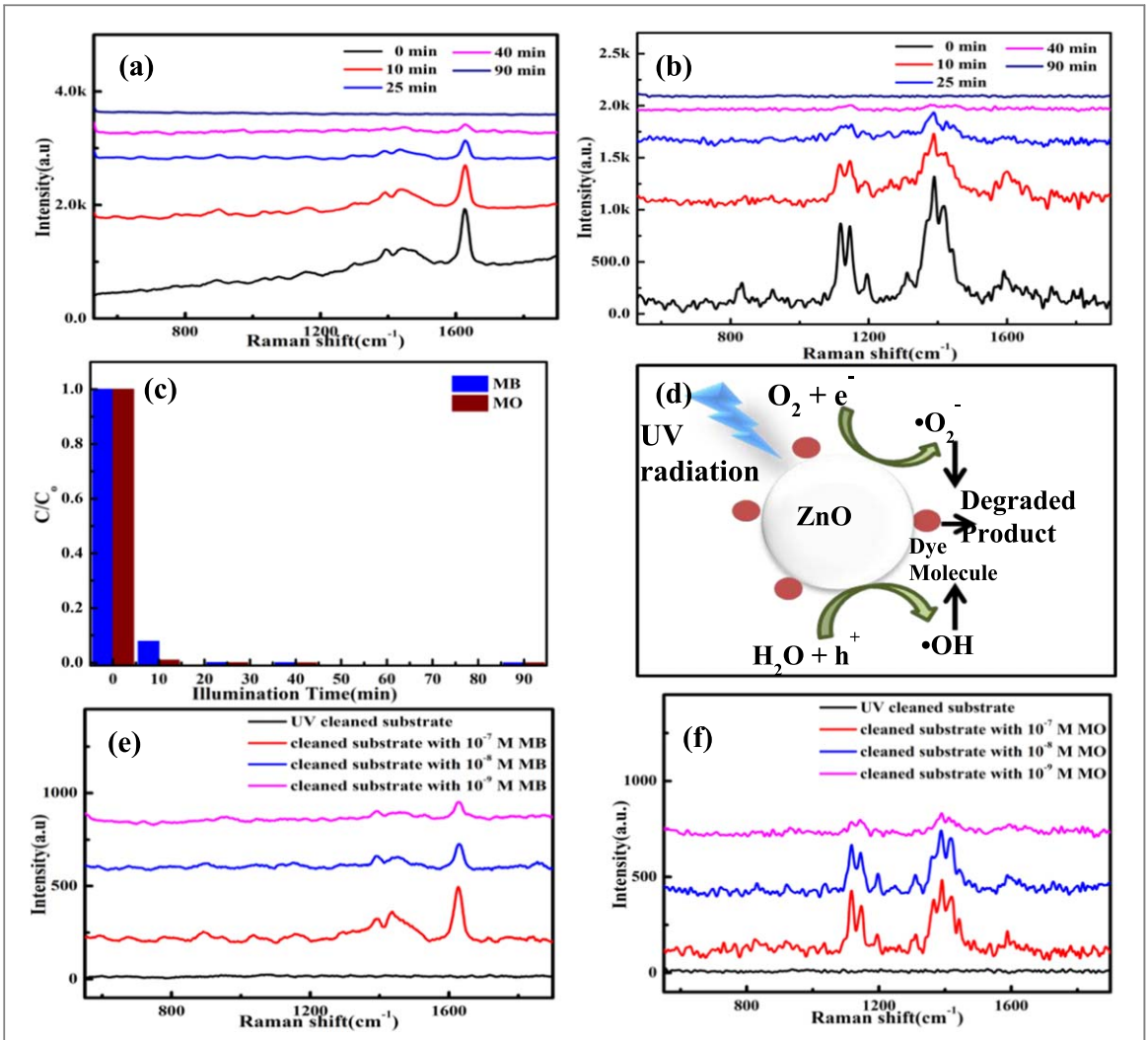

Figure 4. SERS signals for 10^{-5} M concentrations of (a) MB and (b) MO, adsorbed ZnO NPs at different cleaning time (illumination time), (c) Dyes concentrations versus illumination time, (d) Schematic of cleaning mechanism for ZnO NPs based SERS substrate and reusability of ZnO NPs as SERS substrate for (e) MB and (f) MO.

band edges. The enhancement of the Raman signal in the present case can be attributed to the effective charge transfer between adsorbed dye molecules and ZnO NPs, as shown schematically in figure 3(d).

When laser is made to fall on the dye adsorbed ZnO NPs SERS substrate, generation of charge carrier takes place within the HOMO-LUMO of dye molecules and conduction-valence bands of ZnO NPs. These photo-generated charge carriers transfer from the semiconductor band edges to the affinity levels of the adsorbed molecule, which results in an increase in rate of change of polarizability for few vibrational modes of molecules [44–46]. Therefore, the Raman activity as a consequence of the SERS signal is amplified, resulting in significant peak intensity at very low concentrations. The better detectable limit in the present case could be achieved due to the better adsorption of dye molecules over the active surface of well distributed ZnO NPs and hence better charge transfer between them.

The analytical enhancement factor (AEF) for MB and MO adsorbed on ZnO NPs is calculated according to the following equation (4)

$$AEF = (I_{SERS}/I_{NR})(C_{NR}/C_{SERS}) \quad (4)$$

where C_{NR} and C_{SERS} are molar concentration of MB or MO for the normal Raman and SERS and I_{NR} and I_{SERS} are corresponding Raman intensities [20, 44]. In the present case, the AEF of ZnO NPs for detection of MB and MO is found to be around 308 and 116, respectively.

To demonstrate the reusability of used ZnO NPs as a SERS substrate, UV assisted self cleaning of SERS substrate was performed in aqueous medium to remove the adsorbed dye molecules over ZnO NPs so as to make it ready for repeated cycles of detection. The SERS peaks at around 1626 cm^{-1} was chosen for MB (figure 4(a)) and 1390 cm^{-1} was chosen for MO (figure 4(b)) to examine the concentrations of remaining dye molecules over the surface of ZnO NPs after cleaning process at different intervals. The decreased intensity of 1626 cm^{-1} and

1390 cm^{-1} peaks with illuminated time suggests the reduced dye concentration due to effective photo-degradation of adsorbed dye molecules over ZnO NPs leading to the regeneration of the SERS substrate for multiple reuses. The actual concentration of remaining adsorbed dye molecules was calculated using calibration curves of figure 3(c) for respective dyes. The fast decrease in concentration of both the dyes (figure 4(c)) indicates the effective cleaning of ZnO NPs SERS substrate. It shows that maximum cleaning occurs within 25 min of illumination in aqueous medium for both the dyes and the substrate was completely cleaned after 90 min of illumination. Figure 4(d) shows the schematic diagram for possible mechanism for cleaning of adsorbed dye molecules over the surface of ZnO NPs in presence of water. The electron-hole pairs get generated on or near the surface of ZnO NPs under UV illumination. These photo-generated electron-hole pairs react with water and atmospheric or dissolved oxygen and generate hydroxyl radicals (●OH) and superoxide radical anions ($\cdot O_2^-$) respectively [47, 48]. These highly reactive species reacts with adsorbed dye molecules and help in degrading them. This suggests the probable reuse of treated ZnO NPs for SERS application. To demonstrate the reusability of ZnO NPs for SERS application, we used cleaned ZnO NPs for the detection of low concentrations of MB and MO (10^{-9} to 10^{-7} M). The corresponding SERS signals are shown in figures 4(e) and (f), respectively, which indicates nearly same intensities of the SERS peaks for similar concentrations of MB and MO adsorbed over pristine ZnO NPs. This indicates the reusability of ZnO NPs as SERS substrate with repeatable detectability.

4. Conclusion

The bi-functional behaviour of hydrothermally grown ZnO NPs were successfully demonstrated by detection of organic pollutants (MB and MO) using ZnO based SERS substrate and the self cleaning of ZnO based SERS substrate. The detection of nano-molar concentrations of both the organic pollutants (MB and MO) was successfully demonstrated using pristine ZnO NPs over Si as a SERS substrate. This detection limit of ZnO for organic pollutant is the best to our knowledge for any pristine metal oxide nanoparticles as SERS substrate. Further, self cleaning of used ZnO NPs was performed under UV light illumination in aqueous medium for reuse of SERS substrate. The reusability of ZnO based SERS substrate was successfully demonstrated by reemploying the cleaned ZnO NPs for the detection of MB and MO with repeated detectability.

Acknowledgments

The authors thank the support of IIT BHU, its Central Instrument Facility and departmental research facility. Bhawna acknowledges the support of DST, India for PhD INSPIRE fellowship. AKM acknowledges the support of SERB and DST, India for grants no.ECR/2017/000558 and IFA14-MS25. Authors are thankful to Prof. R. Prakash, SMST, IIT(BHU)) for providing UV–vis measurement facility.

ORCID iDs

Ashish Kumar Mishra https://orcid.org/0000-0003-0192-7417

References

[1] Yun S, Lee D, Kim B and Cho C 2019 Highly manufacturable nanoporous ag films using new sputtering system for surface enhanced raman scattering substrate *J Nanosci and Nanotechno* **19** 6429–36
[2] Zhang X S, Meng B, Zhu F Y, Tang W and Zhang H X 2014 Switchable wetting and flexible SiC thin film with nanostructures for microfluidic surface-enhanced Raman scattering sensors *Sensor Actuat A-Phys* **208** 166–73
[3] Wu G, Cao F, Zhao P, Li Z, Yu N, Wang Z, Zhang X, Hu Y, Zhang X and Gu H 2019 Influence of structural parameters on the surface enhanced raman scattering of Au nanoarrays *J Nanosci and Nanotechno* **19** 5317–22
[4] Mishra S, Majee B P, Maurya P K and Mishra A K 2019 Multifunctional low temperature reduced graphite oxides for high performance supercapacitors and SERS applications *Mater. Res. Express* **6** 085527
[5] Vinod T P, Zarzhitsky S, Morag A, Zeiri L, Levi-Kalisman Y, Rapaport H and Jelinek R 2013 Transparent, conductive, and SERS-active Au nanofiber films assembled on an amphiphilic peptide template *Nanoscale* **5** 10487–93
[6] Fan M, Lai F J, Chou H L, Lu W T, Hwang B J and Brolo A G 2013 Surface-enhanced Raman scattering (SERS) from Au: Ag bimetallic nanoparticles: the effect of the molecular probe *Chem. Sci.* **4** 509–15
[7] Galopin E, Barbillat J, Coffinier Y, Szunerits S, Patriarche G and Boukherroub R 2009 Silicon nanowires coated with silver nanostructures as ultrasensitive interfaces for surface-enhanced Raman spectroscopy *ACS appl mater inter* **1** 1396–1403
[8] Cheng D, He M, Ran J, Cai G, Wu J and Wang X 2018 Depositing a flexible substrate of triangular silver nanoplates onto cotton fabrics for sensitive SERS detection *Sensor Actuat B-Chem* **270** 508–17
[9] Zhang K, Zeng T, Tan X, Wu W, Tang Y and Zhang H 2015 A facile surface-enhanced Raman scattering (SERS) detection of rhodamine 6G and crystal violet using Au nanoparticle substrates *Appl. Surf. Sci.* **347** 569–73
[10] Chung E, Gao R, Ko J, Choi N, Lim D W, Lee E K, Chang S I and Choo J 2013 Trace analysis of mercury (ii) ions using aptamer-modified Au/Ag core–shell nanoparticles and SERS spectroscopy in a microdroplet channel *Lab Chip* **13** 260–6

[11] Hossain W, Sen C, Sinha C and Sarkar U K 2019 Surface enhanced Raman Scattering study of 1-H-2 (tolylazo) imidazole (TaiH) induced by uncoupled plasmon of silver nano particles *J nanosci and nanotechno* **19** 3583–90

[12] Yang Y, Li Z Y, Yamaguchi K, Tanemura M, Huang Z, Jiang D, Chen Y, Zhou F and Nogami M 2012 Controlled fabrication of silver nanoneedles array for SERS and their application in rapid detection of narcotics *Nanoscale* **4** 2663–9

[13] Shuhai J, Jun W and Yang J 2013 Ordered silver nanoparticle arrays as surface-enhanced Raman spectroscopy substrates for label-free detection of vitamin C in serum *Sensor Actuat A-Phys* **201** 416–20

[14] Xu D, Jiang H, Yang W, Zhang S and Chen J 2018 SERS effect of Rhodamine 6G molecular probe on AgAu alloy nanowire arrays by a solid-state ionics method *Physica E* **102** 132–6

[15] Geng Z, Liu W, Wang X and Yang F 2011 A route to apply Ag nanoparticle array integrated with microfluidic for surface enhanced Raman scattering *Sensor Actuat A-Phys* **169** 37–42

[16] Musumeci A, Gosztola D, Schiller T, Dimitrijevic N M, Mujica V, Martin D and Rajh T 2009 SERS of semiconducting nanoparticles (TiO_2 hybrid composites) *J. Am. Chem. Soc.* **131** 6040–1

[17] Wang Y, Hu H, Jing S, Wang Y, Sun Z, Zhao B, Zhao C and Lombardi J R 2007 Enhanced Raman scattering as a probe for 4-mercaptopyridine surface-modified copper oxide nanocrystals *Anal. Sci.* **23** 787–91

[18] Gong M, Jiang X, Du J, Li X, Han X, Yang L and Zhao B 2015 Anatase TiO_2 nanoparticles with controllable crystallinity as a substrate for SERS: improved charge-transfer contribution *RSC Adv.* **5** 80269–75

[19] Sun Z, Zhao B and Lombardi J R 2007 ZnO nanoparticle size-dependent excitation of surface Raman signal from adsorbed molecules: Observation of a charge-transfer resonance *Appl. Phys. Lett.* **91** 221106

[20] Majee B P, Mishra S, Pandey R K, Prakash R and Mishra A K 2019 Multifunctional few-layer MoS_2 for photodetection and surface-enhanced Raman spectroscopy application with ultrasensitive and repeatable detectability *J. Phys. Chem. C* **123** 18071–8

[21] Wen H A O 1996 Surface enhancement of Raman and absorption spectra from cyanine dye D266 adsorbed on ZnO colloids *Mol. Phys.* **88** 281–90

[22] Wang Y, Ruan W, Zhang J, Yang B, Xu W, Zhao B and Lombardi J R 2009 Direct observation of surface-enhanced Raman scattering in ZnO nanocrystals *J. Raman Spectrosc.* **40** 1072–7

[23] Shi W 2013 SERS from ZnO Nanorod Arrays and its Application for detecting N719 2013 *Seventh Int. Conf. on Sensing Technology (Piscataway, NJ)* (IEEE) pp 444–6

[24] Yang L, Yang Y, Ma Y, Li S, Wei Y, Huang Z and Long N 2017 Fabrication of semiconductor ZnO nanostructures for versatile SERS application *Nanomaterials* **7** 398

[25] Wang X, Shi W, Jin Z, Huang W, Lin J, Ma G, Li S and Guo L 2017 Remarkable SERS activity observed from amorphous ZnO nanocages *Angew. Chem. Int. Ed.* **56** 9851–5

[26] Liu Q, Jiang L and Guo L 2014 Precursor-directed self-assembly of Porous ZnO nanosheets as high-performance surface-enhanced raman scattering substrate *Small* **10** 48–51

[27] Jin L, She G, Wang X, Mu L and Shi W 2014 Enhancing the SERS performance of semiconductor nanostructures through a facile surface engineering strategy *Appl. Surf. Sci.* **320** 591–5

[28] Lee S, Peng J W and Liu C S 2013 Photoluminescence and SERS investigation of plasma treated ZnO nanorods *Appl. Surf. Sci.* **285** 748–54

[29] Liu L, Pan F, Liu C, Huang L, Li W and Lu X 2018 TiO_2 nanofoam–nanotube array for surface-enhanced Raman Scattering *ACS Appl. Nano Mater.* **1** 6563–6

[30] Shan Y, Zheng Z, Liu J, Yang Y, Li Z, Huang Z and Jiang D 2017 Niobium pentoxide: a promising surface-enhanced Raman scattering active semiconductor substrate *NPJ Comput. Mater.* **3** 11–8

[31] Zhang Q, Li X, Ma Q, Zhang Q, Bai H, Yi W, Liu J, Han J and Xi G 2017 A metallic molybdenum dioxide with high stability for surface enhanced Raman spectroscopy *Nat. Commun.* **8** 14903

[32] Bhawna M B P, Choudhary V, Prakash R and Mishra A K 2019 Hydrothermally grown ZnO nanoparticles for photodegradation of textile dye *AIP Conf. Proc.* 2100020073

[33] Bu T, Ma X, Zhao B and Song W 2018 Facile synthesis of C_3N_4/Ag composite nanosheets as SERS substrate for monitoring the catalytic degradation of methylene blue *Chem. Res. Chin. Univ.* **34** 290–5

[34] Song W, Yang Z, Ma F, Chi M, Zhao B and Lu X 2017 Electrospun magnetic $CoFe_2O_4$/Ag hybrid nanotubes for sensitive SERS detection and monitoring of the catalytic degradation of organic pollutants *RSC Adv.* **7** 40334–41

[35] Cullity B D (ed) 2001 *Elements of X-Ray Diffraction* (Reading, MA: Addison-Wesley)

[36] Rogers K D and Daniels P 2002 An x-ray diffraction study of the effects of heat treatment on bone mineral microstructure *Biomaterials* **23** 2577–85

[37] Zak A K, Majid W A, Abrishami M E and Yousefi R 2011 X-ray analysis of ZnO nanoparticles by Williamson–Hall and size–strain plot methods *Solid State Sci.* **13** 251–6

[38] Scepanovic M G B M, Grujic-Brojcin M, Vojisavljevic K, Bernik S and Sreckovic T 2010 Raman study of structural disorder in ZnO nanopowders *J. Raman Spectrosc.* **41** 914–21

[39] Samanta P K 2017 Review on wet chemical growth and anti-bacterial activity of zinc oxide nanostructures *J Tissue Sci. Eng.* **8** 1000197

[40] Manoj K, Gayathri S, Jayabal P and Ramakrishnan V 2015 Synthesis and characterization of Ni/Ag nanocomposite for surface enhanced Raman scattering measurement *Mater. Res. Express* **2** 065003

[41] Pal S, Depero L E and Alessandri I 2010 Using aggregates of gold nanorods in SERS experiments: an empirical evaluation of some critical aspects *Nanotechnology* **21** 425701

[42] Si M Z, Kang Y P and Zhang Z G 2009 Surface-enhanced Raman scattering (SERS) spectra of Methyl Orange in Ag colloids prepared by electrolysis method *Appl. Surf. Sci.* **255** 6007–10

[43] Lombardi J R and Birke R L 2014 Theory of surface-enhanced Raman scattering in semiconductors *J. Phy. Chem. C* **118** 11120–30

[44] Prakash O, Gautam P, Kumar S, Singh P, Dani R K, Bharty M K, Singh N K, Ghosh A K, Deckert V and Singh R K 2015 Surface enhanced Raman scattering investigation of two novel piperazine carbodithioic acids adsorbed on Ag and ZnO nanoparticles *RSC Adv.* **5** 5571–9

[45] Ji W, Zhao B and Ozaki Y 2016 Semiconductor materials in analytical applications of surface-enhanced Raman scattering *J. Raman Spectrosc.* **47** 51–8

[46] Muehlethaler C, Considine C R, Menon V, Lin W C, Lee Y H and Lombardi J R 2016 Ultrahigh Raman enhancement on monolayer MoS_2 *ACS Photonic* **3** 1164–9

[47] Sinha G, Depero L E and Alessandri I 2011 Recyclable SERS substrates based on Au-coated ZnO nanorods *ACS Appl. Mater. Inter.* **3** 2557–63

[48] Dodd A C, McKinley A J, Saunders M and Tsuzuki T 2006 Effect of particle size on the photocatalytic activity of nanoparticulate zinc oxide *J. Nanopart. Res.* **8** 43